

High-Performance Electrolytic Oxygen Evolution with Seamless Armor Core-Shell FeCoNi Oxynitride

Jun Di,^a Huiyuan Zhu,^b Jiexiang Xia,^{*,a,c} Jian Bao,^a Pengfei Zhang,^c Shi-Ze Yang,^{*,d}
Huaming Li,^a and Sheng Dai^{*,c}

^a School of Chemistry and Chemical Engineering, Institute for Energy Research,
Jiangsu University, 301 Xuefu Road, Zhenjiang, 212013, P. R. China

^b Department of Chemical Engineering, Virginia Tech, Blacksburg, VA, USA

^c Chemical Sciences Division, Oak Ridge National Laboratory, Oak Ridge, USA

^d Materials Science and Technology Division, Oak Ridge National Laboratory, USA

*Corresponding author: xjx@ujs.edu.cn, ananyjlo@gmail.com, dais@ornl.gov

Experimental Section:

Synthesis of FeCoNi oxynitride: 0.2 mmol cobalt acetate, 0.2 mmol nickel acetate and 0.2 mmol iron acetate were dissolved in a mixed solution of 10 mL ethylene glycol and 2 mL H₂O. After stirring for 30 min, the solution was transferred into a 25 ml Teflon-lined autoclave, sealed and heated at 190 °C for 48 h. The product was collected after centrifugation, washed with deionized water and ethanol for several times, and dried at 50 °C. Then, 0.05 g of above powder was calcined at 400 °C for 3 h under the NH₃ atmosphere (500 mL/min) to obtain the FeCoNi oxynitride. For the preparation of monometallic component or bi-metal component, the process was similar only with the using of corresponded metal sources.

Synthesis of CoNi nitride: 0.2 mmol cobalt acetate and 0.2 mmol nickel acetate were dissolved in a mixed solution of 10 mL ethylene glycol and 2 mL H₂O. After stirring for 30 min, the solution was transferred into a 25 ml Teflon-lined autoclave, sealed and heated at 190 °C for 48 h. The product was collected after centrifugation, washed with deionized water and ethanol for several times, and dried at 50 °C. Then, 0.05 g of above powder was calcined at 400 °C for 3 h under the NH₃ atmosphere (500 mL/min) to obtain the CoNi nitride.

Synthesis of Co₂N nitride: 0.2 mmol cobalt acetate was dissolved in a mixed solution of 10 mL ethylene glycol and 2 mL H₂O. After stirring for 30 min, the solution was transferred into a 25 ml Teflon-lined autoclave, sealed and heated at 190 °C for 48 h. The product was collected after centrifugation, washed with deionized water and ethanol for several times, and dried at 50 °C. Then, 0.05 g of above powder was calcined at 400 °C for 3 h under the NH₃ atmosphere (500 mL/min) to obtain the Co₂N.

Synthesis of Ni₃N nitride: 0.2 mmol nickel acetate was dissolved in a mixed solution of 10 mL ethylene glycol and 2 mL H₂O. After stirring for 30 min, the solution was transferred into a 25 ml Teflon-lined autoclave, sealed and heated at 190 °C for 48 h. The product was collected after centrifugation, washed with deionized water and ethanol for several times, and dried at 50 °C. Then, 0.05 g of above powder was calcined at 400 °C for 3 h under the NH₃ atmosphere (500 mL/min) to obtain the Ni₃N.

Hydrogenation of FeCoNi oxynitride: FeCoNi oxynitride was placed in quartz boat and calcined in a tube furnace at 400 °C for 2 h under 5% H₂/Ar mixture gas to achieve the hydrogenation of FeCoNi oxynitride.

Characterizations: The crystal structure of catalysts was characterized by powder X-ray diffraction (XRD) (Shimadzu XRD-6000 diffractometer) using Cu K α irradiation. X-ray photoelectron spectroscopy (XPS) measurements were carried out on a VG MultiLab 2000 system with a monochromatic Mg K α source. Transmission electron microscopy (TEM) was taken with a JEOL-JEM-2100 operating at 200 kV. High-resolution annular dark-field (ADF) imaging and electron energy-loss spectroscopy (EELS) analyses were carried out in aberration-corrected scanning transmission electron microscope Nion Ultra STEM100 at 100 kV and Nion Ultra STEM200 at 200 keV in Oak Ridge National Laboratory. The beam convergent semi-angle was 30 mrad and EELS collection semi-angle was 48 mrad. The energy scale in EELS spectrum is carefully calibrated to get correct quantification results.

Electrochemical Measurements: All of the electrochemical measurements were carried out in a three-electrode system on an electrochemical work station (CHI660E). 4 mg of samples were dispersed in 1 ml of mixed solution (isopropanol/H₂O 1:3 v/v). After the addition of 15 μ L Nafion solution (Sigma Aldrich, 5 wt%), the mixed was sonicated for 30 min to form a homogeneous ink. Then 5 μ L of the dispersion (containing 20 μ g of sample) was loaded onto a glassy carbon electrode with 3 mm diameter (loading \sim 0.284 mg cm⁻²). Finally, the obtained catalyst films were dried at room temperature. Linear sweep voltammetry (LSV) was performed in 1 M KOH solution with a scan rate of 5 mV s⁻¹. The glassy carbon electrode with various catalysts served as the working electrode. A Pt electrode was employed as counter electrode and the Ag/AgCl electrode was acted as reference electrode. Cyclic voltammetry (CV) measurements at 50 mV s⁻¹ were performed for 30 cycles prior to recording LSV for each sample. The measured potentials vs. Ag/AgCl were converted to the reversible hydrogen electrode (RHE) scale according to the Nernst equation: $E_{\text{RHE}} = E_{\text{Ag/AgCl}} + 0.0591 \times \text{pH} + 0.1976$. All the data was obtained without iR correction except for special illustration.

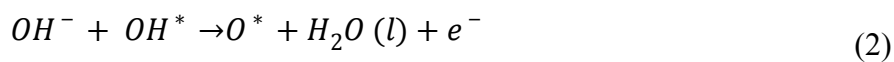
The polarization curves were replotted as overpotential (η) vs. log current (log j) to get Tafel plots for quantification of the OER performances of the obtained catalysts. By fitting the linear portion of the Tafel plots to the Tafel equation ($\eta = b \log(j) + a$), the Tafel slope (b) can be acquired.

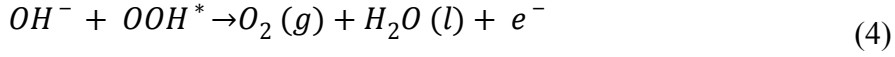
Electrochemical impedance spectroscopy (EIS) measurements of the catalysts were performed using above three electrode systems at overpotential of 0.4 V. The frequency range was 100 K Hz to 1 Hz, and the amplitude of the applied voltage was 5 mV.

The values of TOF were calculated by assuming that every metal atom was involved in the catalysis (lowest TOF limits were calculated): $\text{TOF} = (j \cdot S) / (4 \cdot F \cdot n)$. Here, j (mA cm^{-2}) was the measured current density at $\eta = 0.35$ V, S was the surface area of glassy carbon electrode (0.0707 cm^2), 4 means 4 electrons per O_2 molecular, F was Faraday's constant ($96485.3 \text{ C mol}^{-1}$), and n was the moles of the metal atom on the electrode.

Density functional theory simulation: DFT calculations were performed using the projected augmented wave method (PAW),^[S1, S2] as implemented in Vienna ab-initio simulation package (VASP).^[S3, S4] For the structural relaxation and electronic-structure calculations, the generalized gradient approximation (GGA) method was used with the Perdew–Burke–Ernzerhof (PBE) exchange-correlation functional.^[S5] The electron wave function was expanded in a plane-wave basis set with an energy cutoff of 500 eV. Vacuum space of about 12 Å was used in the z-direction to avoid the interaction between periodic images. The convergence criteria for structural optimization and energy on each atom were set to 0.02 eV/Å and 10^{-4} eV, respectively.

The free energy diagram was calculated according to methods reported before.^[S6] The OER reaction pathway can be written as follows:





The symbol of “*” signifies the adsorption site on the surface, (g) and (l) represent the phases. The free energy ΔG of each step is obtained by the following equation:

$$\Delta G = \Delta E + \Delta ZPE - T\Delta S + \Delta G_U + \Delta G_{PH},$$

Where ΔE , ΔZPE , and ΔS represents the different intermediate energy, zero-point energy changes and entropy of the reaction, respectively. ΔE is obtained from DFT calculations, while ΔZPE and ΔS are adopted from the values in reference. ΔG_U and ΔG_{PH} are effects due to applied bias and solution pH level and we set those to zero to simplify the analysis. Each step of ΔG is obtained by:

$$\Delta G_{OH} = G(OH^*) - G(*) - G(H_2O) + \frac{1}{2}G(H_2)$$

$$\Delta G_O = G(O^*) - G(OH^*) + \frac{1}{2}G(H_2)$$

$$\Delta G_{OOH} = G(OOH^*) - G(O^*) - G(H_2O) + \frac{1}{2}G(H_2)$$

The binding energy of related species are defined by:^[6]

$$\Delta E_{OH^*} = E(OH^*) - E(*) - (E_{H_2O} - \frac{1}{2}E_{H_2})$$

$$\Delta E_{O^*} = E(O^*) - E(*) - (E_{H_2O} - E_{H_2})$$

$$\Delta E_{OOH^*} = E(OOH^*) - E(*) - (2E_{H_2O} - \frac{3}{2}E_{H_2})$$

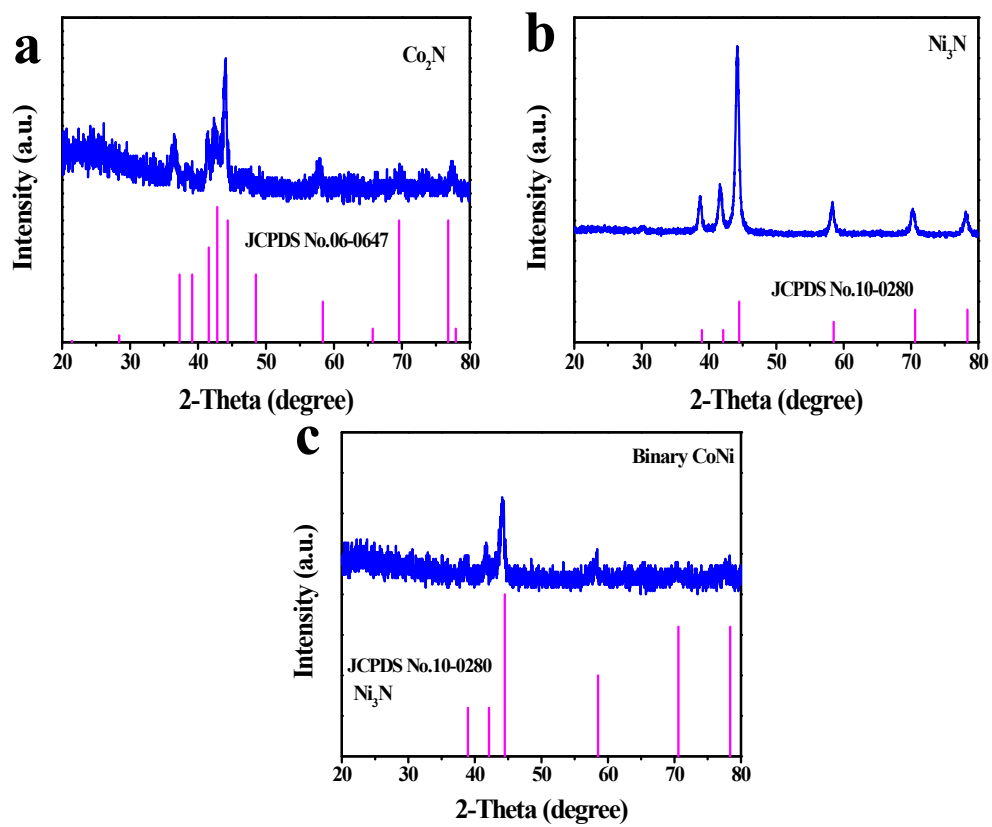


Figure S1. XRD patterns for (a) Co_2N , (b) Ni_3N , (c) binary CoNi.

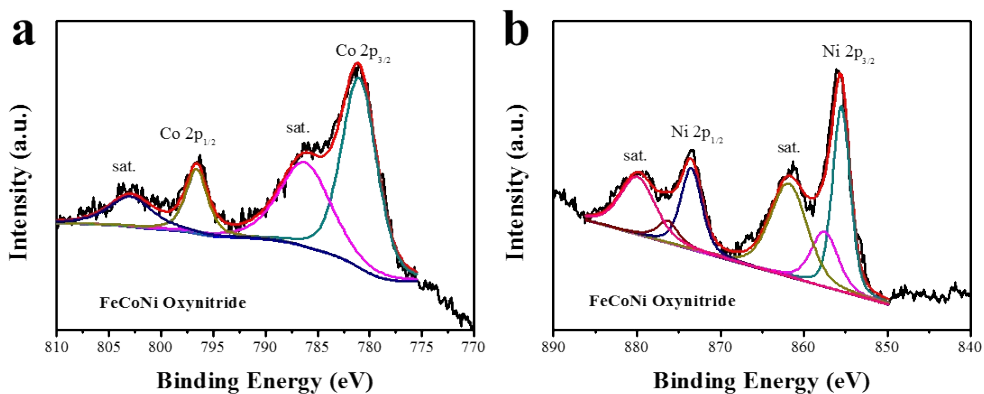


Figure S2. Fitted XPS spectra of (a) Co 2p, (b) Ni 2p in FeCoNi oxynitride.

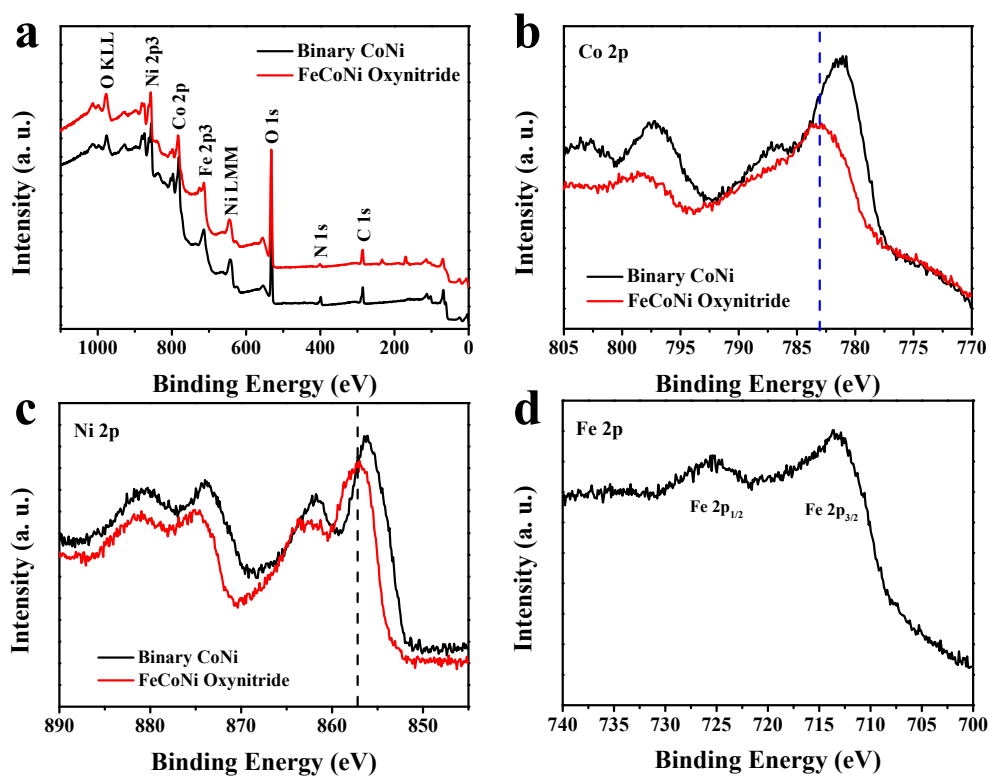


Figure S3. XPS spectra of (a) full scan, (b) Co 2p, (c) Ni 2p, (d) Fe 2p.

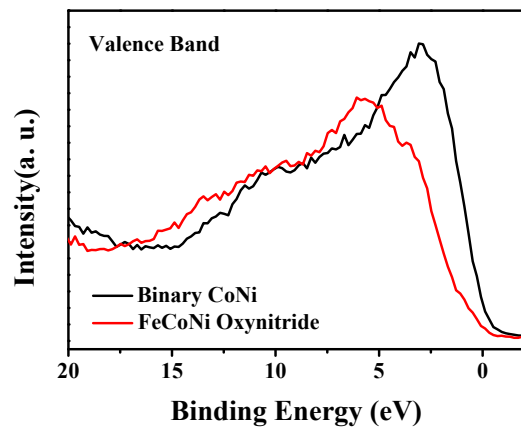


Figure S4. Valence band spectra of binary CoNi and FeCoNi oxynitride.

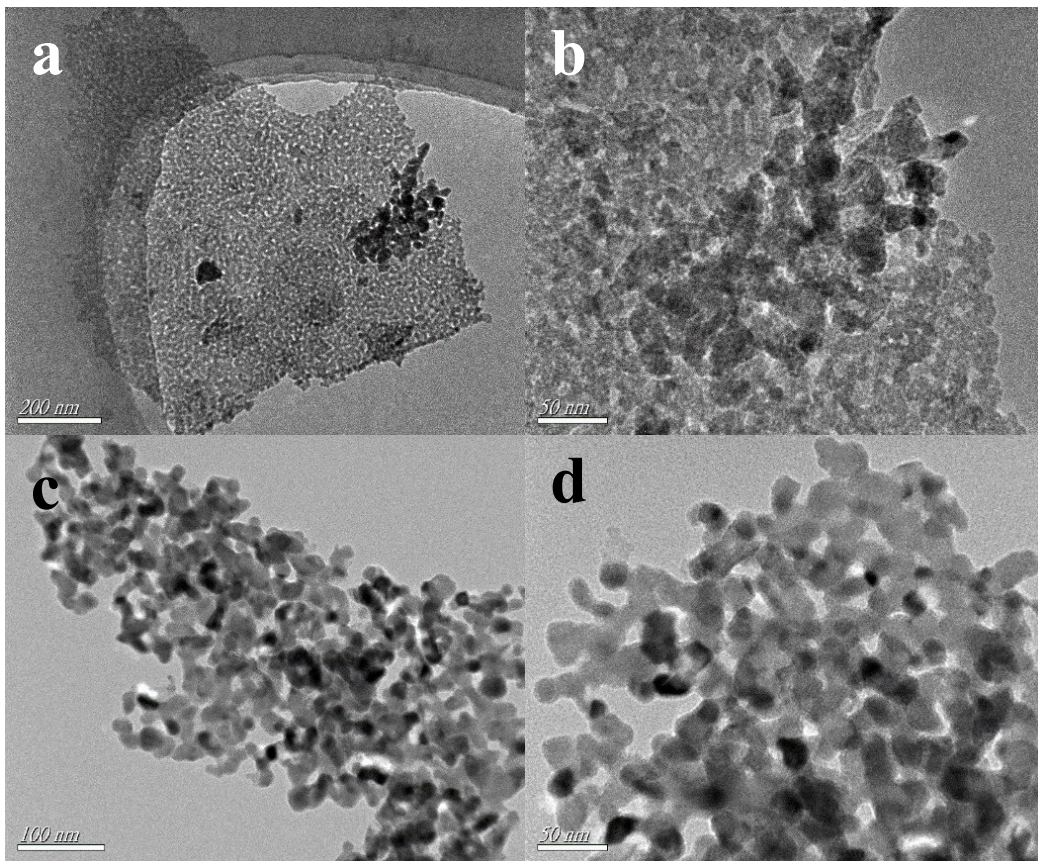


Figure S5. TEM images of Co_2N (a), (b) and Ni_3N (c), (d).

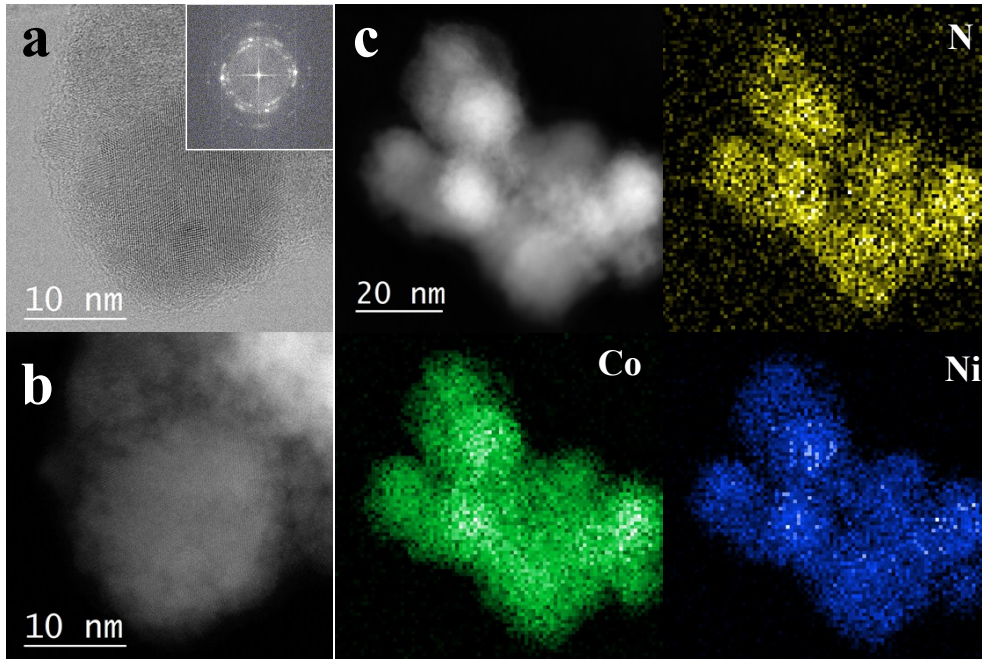


Figure S6. The TEM and EELS images of the CoNi nitride.

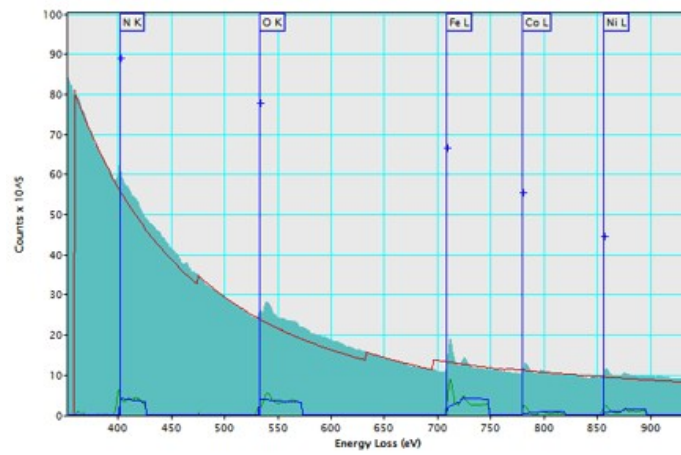


Figure S7. EELS of FeCoNi oxynitride.

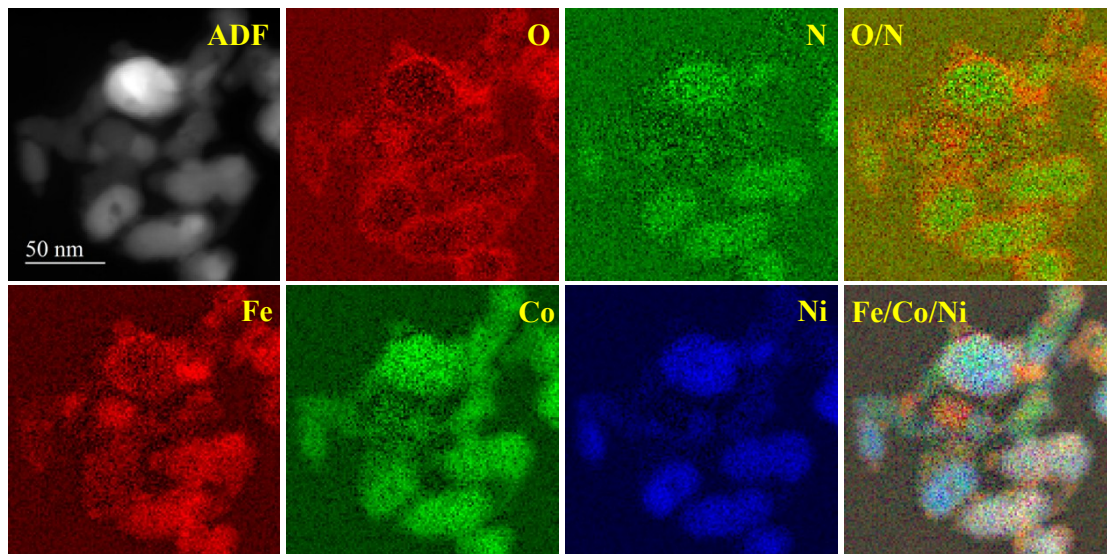


Figure S8. Electron energy loss mapping of nitride-core-oxide-shell FeCoNi oxynitride nanoparticles using area density of elements.

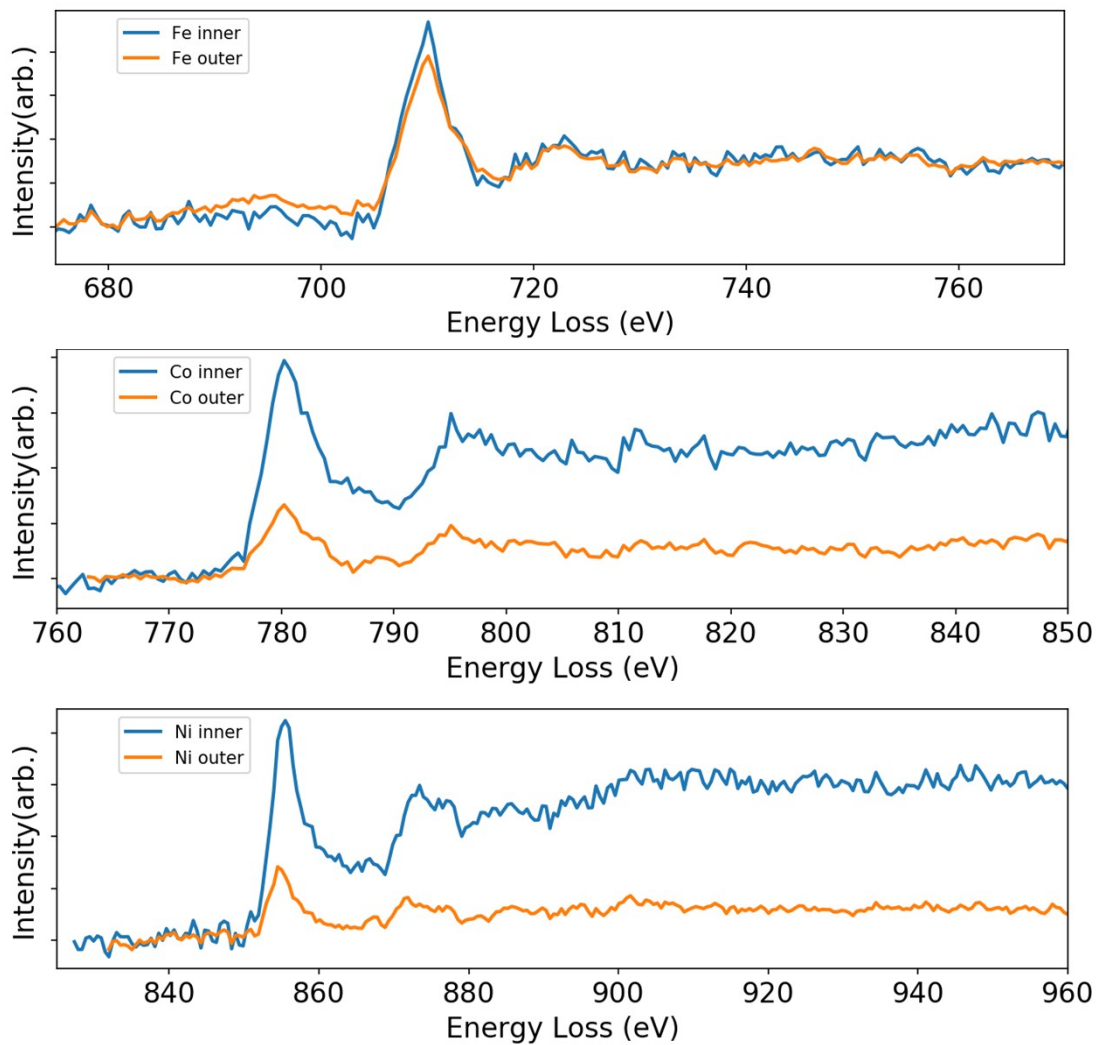


Figure S9. EELS K-edge fingerprint spectrum of both inner and outer of FeCoNi oxynitride.

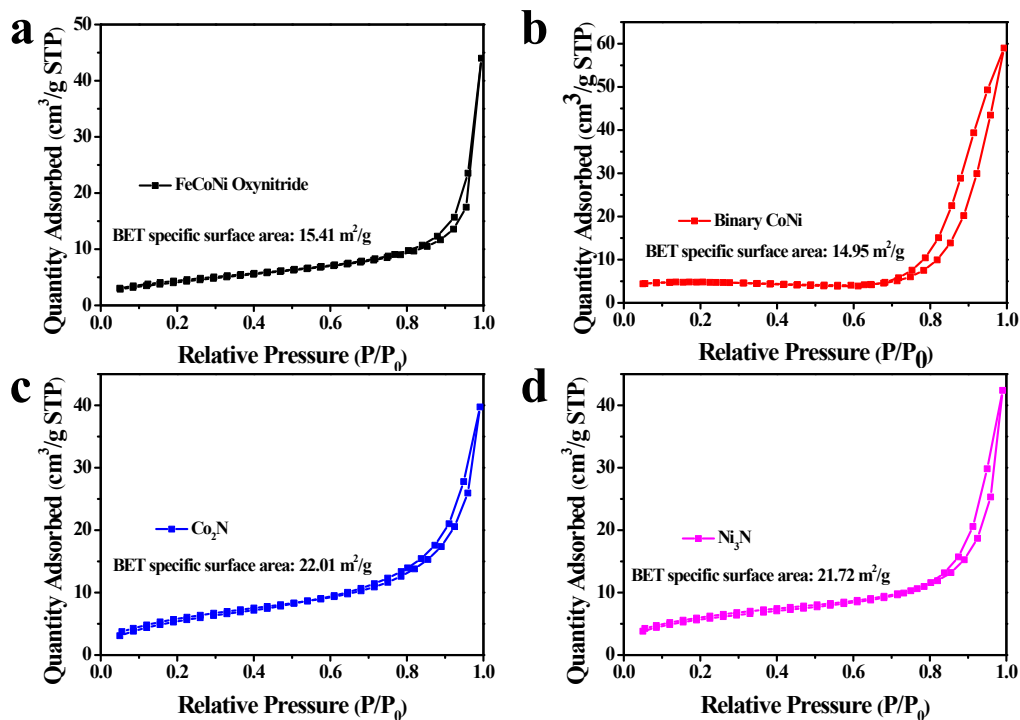


Figure S10. Nitrogen absorption-desorption isotherms of (a) FeCoNi oxynitride, (b) binary CoNi, (c) Co₂N, (d) Ni₃N.

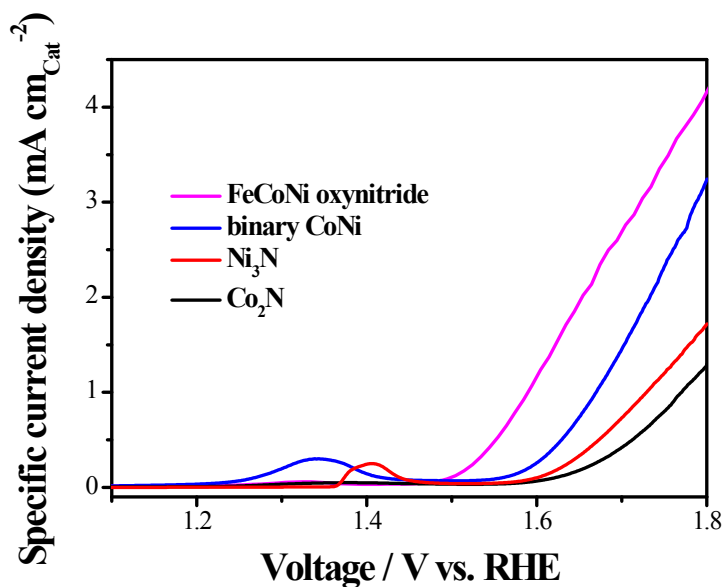


Figure S11. The normalized polarization curves of FeCoNi oxynitride, binary CoNi, Ni₃N, Co₂N by the BET surface area of electrocatalysts.

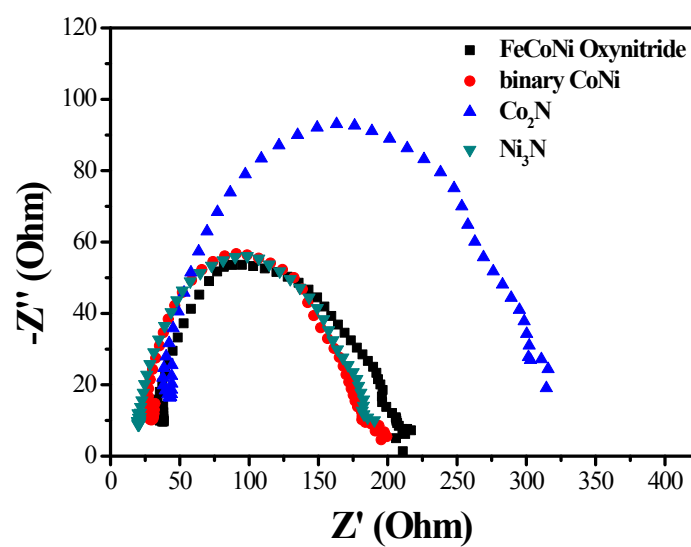


Figure S12. Electrochemical impedance spectroscopy for the FeCoNi oxynitride, binary CoNi, Co_2N and Ni_3N composite.

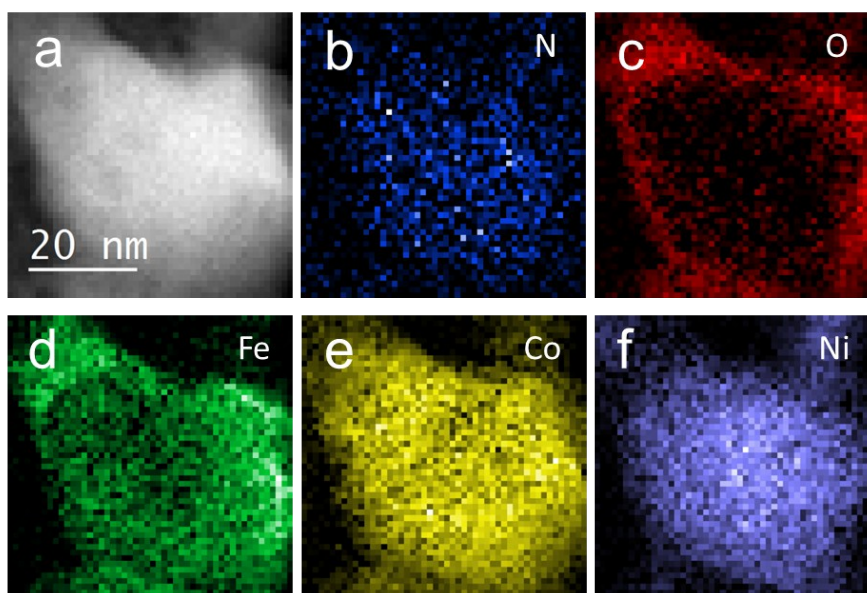


Figure S13. (a) HAADF-STEM image, and (b-f) the corresponding EELS elemental mappings of FeCoNi oxynitride nanoparticle after cycle.

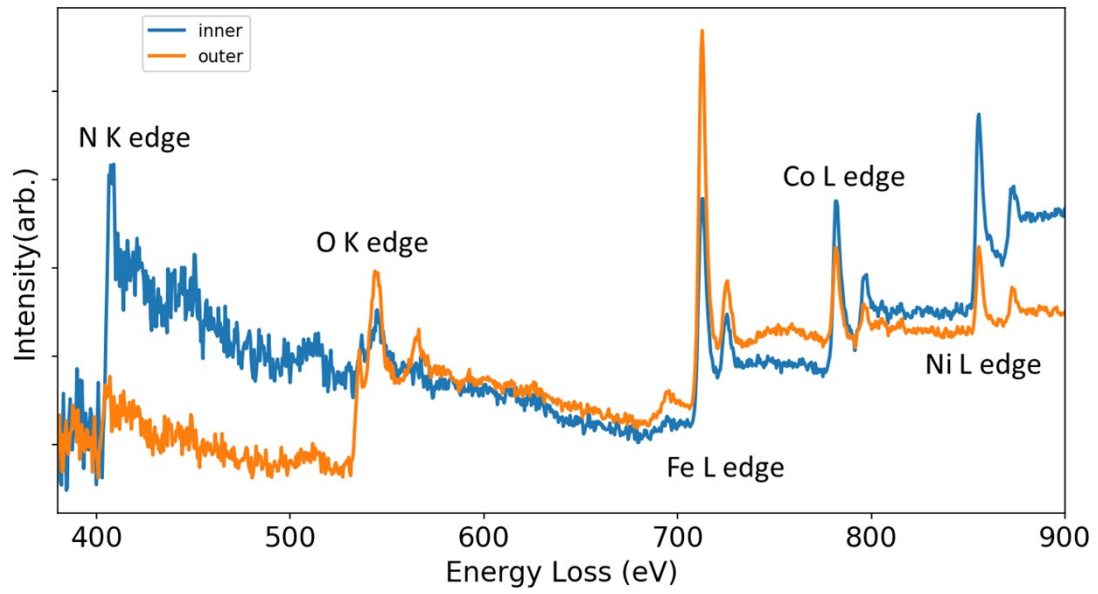


Figure S14. EELS spectrum of both inner and outer of FeCoNi oxynitride after stability test.

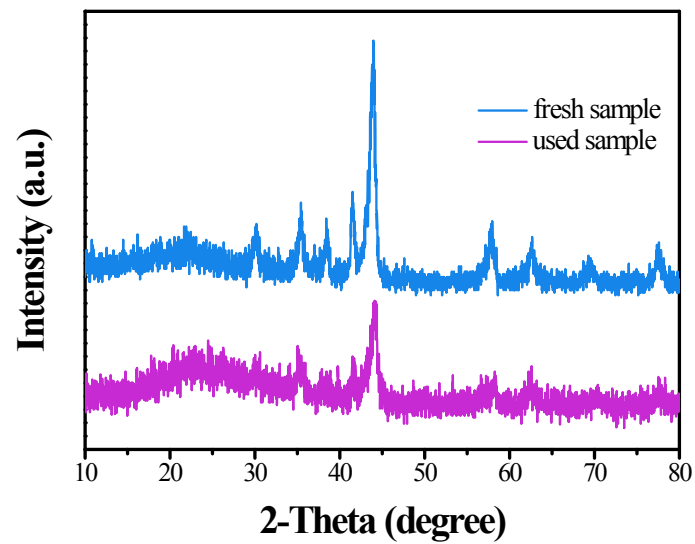


Figure S15. XRD patterns of the FeCoNi oxynitride before and after the cycling experiments.

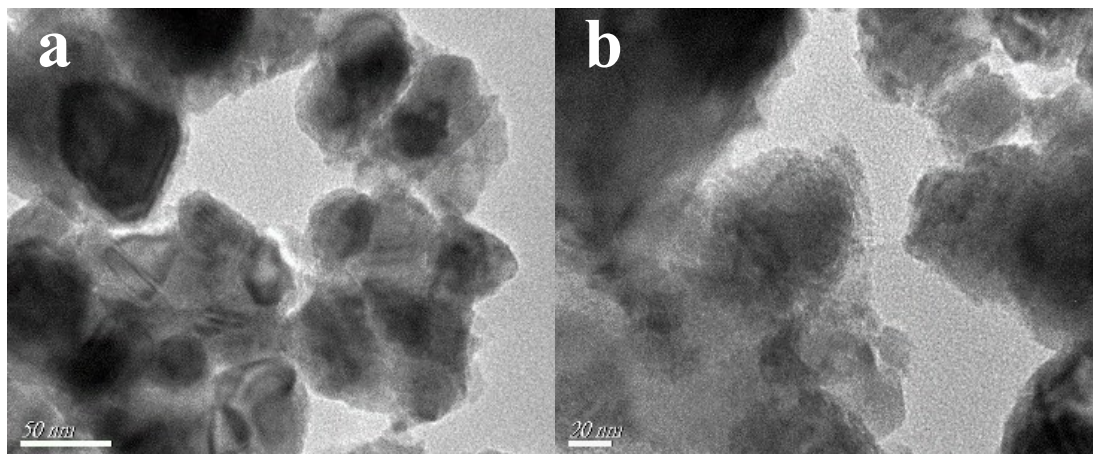


Figure S16. The TEM images of the FeCoNi oxynitride after hydrogenation.

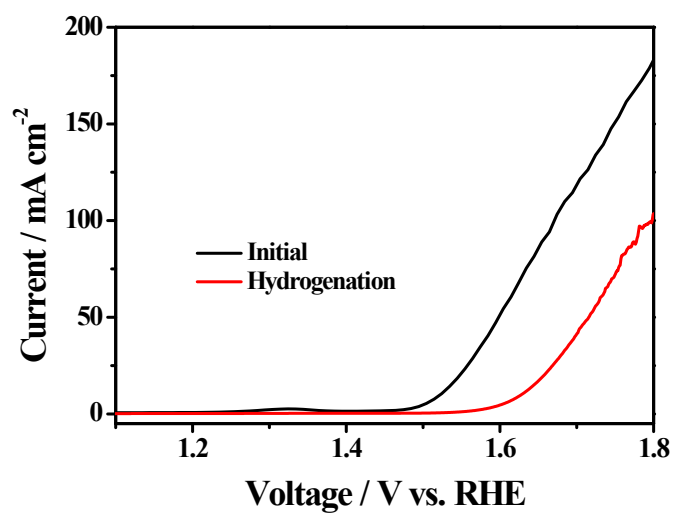


Figure S17. The comparison of polarization curves of the FeCoNi oxynitride before and after hydrogenation.

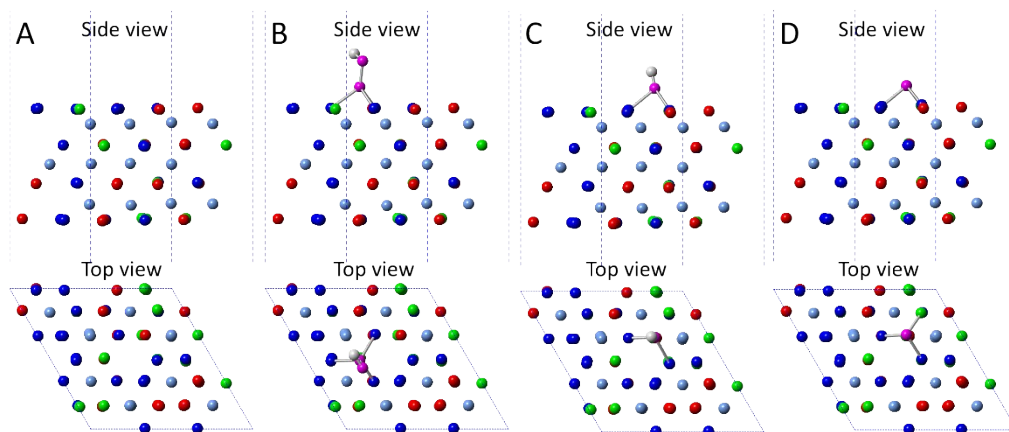


Figure S18. Adsorption structures on Ni_3N alloy. A, structure with vacant adsorption sites *; B, structure with OOH^* ; C, structure with OH^* ; D, structure with O^* .

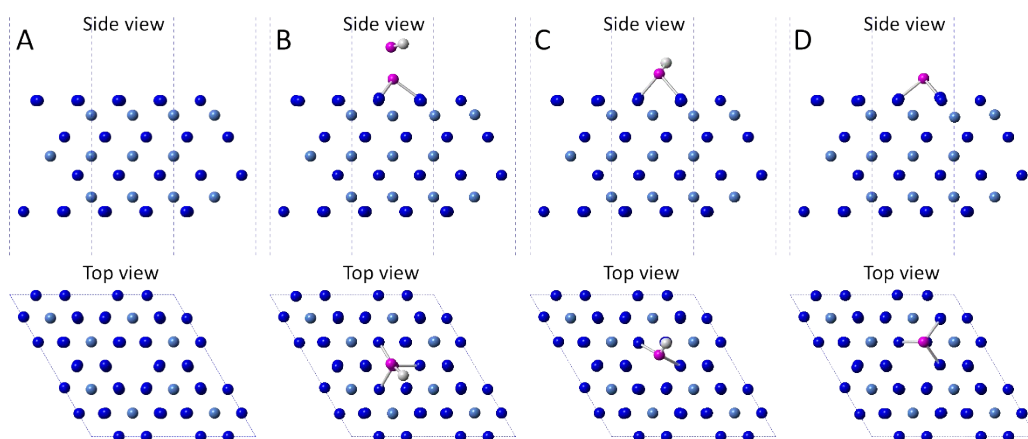


Figure S19. Adsorption structures on Ni_3N . A, structure with vacant adsorption sites *; B, structure with OOH^* ; C, structure with OH^* ; D, structure with O^* .

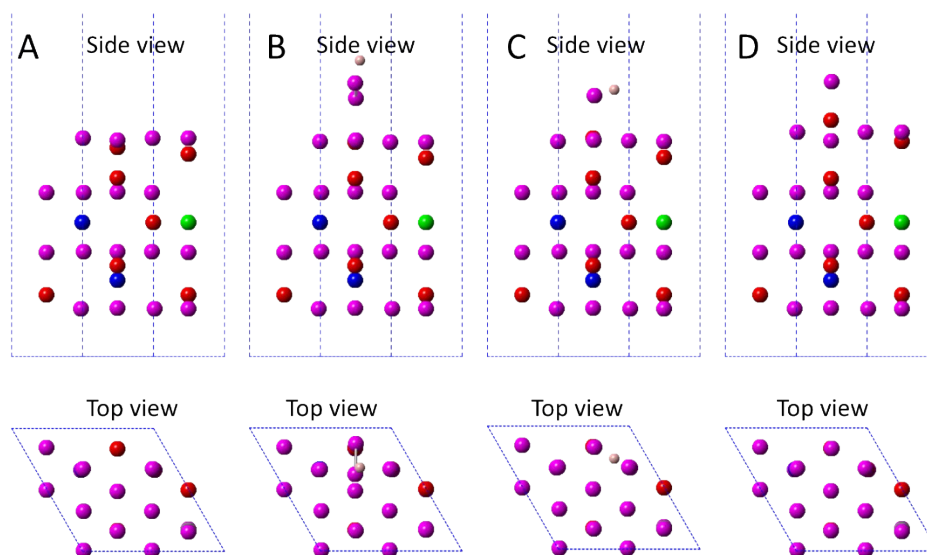


Figure S20. Adsorption structures on Fe_3O_4 surface. A, structure with vacant adsorption sites *; B, structure with OOH^* ; C, structure with OH^* ; D, structure with O^* .

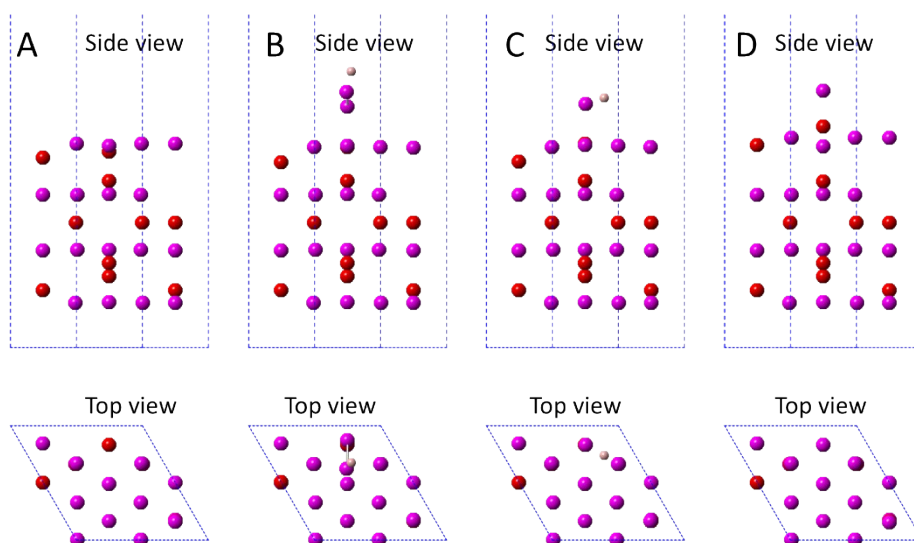


Figure S21. Adsorption structures on Fe_3O_4 surface doped with Co and Ni. A, structure with vacant adsorption sites *; B, structure with OOH^* ; C, structure with OH^* ; D, structure with O^* .

Table S1. Chemical compositions of nitride cores with average chemical formula $\text{Fe}_{0.70}\text{Co}_{0.56}\text{Ni}_{0.92}\text{N}_{1.0}\text{O}_{0.06}$.

Elements	Particle 1	Particle 2	Particle 3	Particle 4	Result	Error
<i>N</i>	1.00	1.00	1.00	1.00	1.00	0.00
O	0.02	0.00	0.14	0.09	0.06	0.06
Fe	0.56	0.32	0.98	0.96	0.70	0.32
Co	0.69	0.61	0.49	0.43	0.56	0.12
Ni	0.96	1.05	0.86	0.81	0.92	0.11

Table S2. Chemical compositions of oxide shells with average chemical formula $\text{Fe}_{0.48}\text{Co}_{0.1}\text{Ni}_{0.21}\text{N}_{0.05}\text{O}_{1.0}$.

Elements	Particle 1	Particle 2	Particle 3	Particle 4	Result	Error
<i>N</i>	0.09	0.00	0.06	0.06	0.05	0.04
O	1.00	1.00	1.00	1.00	1.00	0.00
Fe	0.54	0.38	0.48	0.50	0.48	0.07
Co	0.14	0.09	0.08	0.10	0.10	0.03
Ni	0.31	0.10	0.22	0.20	0.21	0.09

Table S3. L_3/L_2 ratios of Fe, Co, Ni in raw FeCoNi oxynitride and after reaction.^[S7-S9]

	L_3/L_2 ratios	Fe	Co	Ni
Raw material	core	2.86	2.82	2.18
	shell	3.03	1.59	1.78
After reaction	core	3.14	1.82	2.51
	shell	3.89	2.31	1.75

Table S4. Comparison of the electrocatalytic activity of FeCoNi oxynitride to recently reported catalysts for OER in basic solutions.

Electrocatalysts	Electrolytes	Overpotential (mV) at 10 mA cm ⁻²	Mass loading (mg cm ⁻²)	Substrate	Reference
FeCoNi oxynitride	1 M KOH	291	0.284	GCE	This work
FeCoW oxyhydroxides	1 M KOH	223	0.21	GCE	Science 2016, 352, 333
NiFe LDH	1 M NaOH	240	-	Ni foam	Science 2014, 345, 1593
CeO _x /CoS	1 M KOH	269	0.2	GCE	Angew. Chem. Int. Ed. 2018, 57, 8654
p-Cu _{1-x} NNi _{3-y} /FeNiCu	1 M KOH	280	0.367	GCE	Nat. Commun. 2018, 9, 2326
Ni ₂ P	1 M KOH	290	0.14	GCE	Energy Environ. Sci. 2015, 8, 2347
Co ₃ O ₄ /Co-Fe oxide double-shelled nanoboxes	1 M KOH	297 after iR correction	0.255	GCE	Adv. Mater. 2018, 30, 1801211
NiFe LDH	1 M KOH	300	0.07	GCE	J. Am. Chem. Soc. 2015, 137, 1305
NiFe-LDH single-layer nanosheets	1 M KOH	302	0.07	GCE	Nat. Commun. 2014, 5, 4477
porous Co phosphide/Co phosphate thin film	1 M KOH	305 after iR correction	0.1	-	Adv. Mater. 2015, 27, 3175
Ni ₃ Se ₂	0.3 M KOH	310	0.217	GCE	Energy Environ. Sci. 2016, 9, 1771
Ni _{0.2} Co _{0.3} Ce _{0.5} O _x	1 M NaOH	310	-	GCE	Energy Environ. Sci. 2014, 7, 682
monolayer Ni _{0.75} V _{0.25} -LDH	1 M KOH	318	0.141	GCE	Nat. Commun. 2016, 7, 11981
NiCo ₂ O ₄ ultrathin nanosheets	1 M KOH	320	0.285	GCE	Angew. Chem. Int. Ed. 2015, 54, 7399
CoMn LDH	1 M KOH	324	0.142	GCE	J. Am. Chem. Soc. 2014, 136, 16481
CoMnP nanoparticles	1 M KOH	330	0.284	GCE	J. Am. Chem. Soc. 2016, 138, 4006
α-Ni(OH) ₂	0.1 M KOH	331 after iR correction	0.2	GCE	J. Am. Chem. Soc. 2014, 136, 7077
Co ₃ O ₄ /NiCo ₂ O ₄ double-shelled nanocages	1 M KOH	340	1	Ni foam	J. Am. Chem. Soc. 2015, 137, 5590
Ni-Co oxide hierarchical nanosheets	1 M NaOH	340	-	FTO	Adv. Energy Mater. 2015, 5, 1500091
LiCo _{0.8} Fe _{0.2} O ₂	0.1 M KOH	340 after iR correction	0.464	GCE	Adv. Mater. 2015, 27, 7150
single-unit-cell CoSe ₂ sheets	1 M KOH	345	0.17	GCE	Angew. Chem. Int. Ed. 2015, 54, 12004
CoP _x film	1 M KOH	345	2.71	Cu foil	Angew. Chem. Int. Ed. 2015, 54, 6251
NiCo _{2.7} (OH) _x	1 M KOH	350 after iR correction	0.2	GCE	Adv. Energy Mater. 2015, 5, 1401880
NiCo ₂ O ₄ nanowires	1 M KOH	360 after iR correction	0.3	Ti mesh	Adv. Energy Mater. 2015, 5, 1402031
La _{0.5} Sr _{1.5} Ni _{1-x} Fe _x O _{4±δ} oxides	0.1 M KOH	360 after iR correction	0.051	GCE	Nat. Commun. 2018, 9, 3150
hollow Co ₃ S ₄ nanosheets	0.1 M KOH	363 after iR correction	0.283	GCE	ACS Nano 2014, 8, 10909
exfoliated NiCo LDH	1 M KOH	367	0.17	Carbon paper	Nano Lett. 2015, 15, 1421
Co ₃ O ₄ nano-islands	1 M NaOH	376	0.0047	FTO	Adv. Energy Mater. 2016, 6, 1600697
Co ₂ B	0.1 M KOH	380 after iR correction	0.21	GCE	Adv. Energy Mater. 2016, 6, 1502313
Ni-Co mixed oxide cages	1 M KOH	380 after iR correction	-	GCE	Adv. Mater. 2016, 28, 4601
BP/Co ₂ P	1 M KOH	380 after iR correction	0.14	GCE	Angew. Chem. Int. Ed. 2018, 57, 2600
Au@Co ₃ O ₄ nanocrystals	0.1 M KOH	385 after iR correction	0.2	GCE	Adv. Mater. 2014, 26, 3950
Co ₂ (μ-OH) ₂ (bbta)	1 M KOH	387	0.18	GCE	J. Am. Chem. Soc. 2016, 138, 8336
FeNC sheets/NiO	0.1 M KOH	390	0.24	GCE	Angew. Chem. Int. Ed. 2015, 54, 10530
Mesoporous MnCo ₂ O ₄	0.1 M KOH	400	-	GCE	Angew. Chem. Int. Ed. 2017, 56, 14977
reduced mesoporous Co ₃ O ₄ nanowires	1 M KOH	405 after iR correction	0.136	GCE	Adv. Energy Mater. 2014, 4, 1400696
O-NiCoFe-LDH	0.1 M KOH	420	0.12	RDE	Adv. Energy Mater. 2015, 5, 1500245

FeS _x	0.1 M KOH	420 after iR correction	-	FTO	Adv. Energy Mater. 2016, 6, 1502095
nanosized LaCoO ₃	0.1 M KOH	490	0.25	GCE	Nat. Commun. 2016, 7, 11510
Fe-Ni@NC-CNTs	1 M KOH	274	0.5	GCE	Angew. Chem. Int. Ed. 2018, 57, 8921
cobalt-based borate (Co-Bi) ultrathin nanosheets/graphene	1 M KOH	290	0.285	GCE	Angew. Chem. Int. Ed. 2016, 55, 2488
C-Ni ₃ P ₄ -Ni ₂ P	1 M KOH	300	0.2	GCE	Energy Environ. Sci. 2016, 9, 1246
Co ₃ O ₄ /rm-GO	1 M KOH	310	0.24	GCE	Nat. Mater. 2011, 10, 780
CoP/N-doped carbon nanotube hollow polyhedron	1 M KOH	310	0.4	GCE	J. Am. Chem. Soc. 2018, 140, 2610
Ni ₃ C/C	1 M KOH	316	0.285	GCE	Adv. Mater. 2016, 28, 3326
Ni-/Co-porphyrin multilayers on rGO	1 M KOH	330	0.0127	RDE	Chem. Sci. 2016, 7, 5640
NiFe LDHs/ nitrogen-doped graphene framework	0.1 M KOH	337 after iR correction	0.25	GCE	Adv. Mater. 2015, 27, 4516
CoP/rGO	1 M KOH	340	0.28	GCE	Chem. Sci. 2016, 7, 1690
3D crumpled graphene-CoO	1 M KOH	340	0.707	GCE	Energy Environ. Sci. 2014, 7, 609
Fe ₃ O ₄ @Co ₉ S ₈ /rGO	1 M KOH	340 after iR correction	0.25	GCE	Adv. Funct. Mater. 2016, 26, 4712
nitrogen-doped reduced graphene oxides-CoSe ₂	0.1 M KOH	366	0.2	GCE	ACS Nano 2014, 8, 3970
Co ₃ O ₄ /N-doped porous carbon	0.1 M KOH	390 after iR correction	0.364	GCE	Nano Energy 2015, 12, 1
Ni/N/C paper	0.1 M KOH	390 after iR correction	0.4	GCE	Adv. Energy Mater. 2015, 5, 1401660
N-doped Co ₉ S ₈ /graphene	0.1 M KOH	409 after iR correction	0.2	GCE	Energy Environ. Sci. 2016, 9, 1320
Co single atom/CNT	0.1 M KOH	410 after iR correction	0.05	GCE	Angew. Chem. Int. Ed. 2018, 57, 3514
ZnCo ₂ O ₄ /N-doped-CNT	0.1 M KOH	420	0.2	GCE	Adv. Mater. 2016, 28, 3777
Mn _{0.1} Ni ₁ /nitrogen doped carbon	0.1 M KOH	420 after iR correction	0.28	GCE	Adv. Funct. Mater. 2015, 25, 393
Co ₉ S ₈ @MoS ₂ /carbon nanofibers	1 M KOH	430 after iR correction	0.212	GCE	Adv. Mater. 2015, 27, 4752
nitrogen-doped graphene/cobalt-embedded porous carbon polyhedron	0.1 M KOH	430 after iR correction	0.354	GCE	Adv. Funct. Mater. 2015, 25, 872
Co ₃ O ₄ /nitrogen-doped, partially graphitized carbon framework	0.1 M KOH	450	0.204	GCE	Angew. Chem. Int. Ed. 2016, 55, 4977
N, S codoped graphite foam	1 M KOH	346 after iR correction	-	-	Adv. Energy Mater. 2016, 6, 1501492
sulfur-doped carbon nanotube-graphene nanolobe	1 M KOH	350 after iR correction	0.23	pyrolytic graphite electrode	Adv. Energy Mater. 2016, 6, 1501966
nitrogen doped graphene nanoribbon networks	1 M KOH	360	0.5	GCE	Sci. Adv. 2016, 2, e1501122
g-C ₃ N ₄ -CNTs	0.1 M KOH	370	0.204	GCE	Angew. Chem. Int. Ed. 2014, 53, 7281
N-doped carbon nanotube frameworks	1 M KOH	370	0.2	GCE	Nature Energy 2016, 1, 15006
nitrogen-doped carbon	0.1 M KOH	380	0.2	GCE	Nature Commun. 2013, 4, 2390
N ₃ P ₂ O tri-doped porous graphite carbon@oxidized carbon cloth	1 M KOH	410	-	-	Energy Environ. Sci. 2016, 9, 1210
Ti ₃ C ₂ /g-C ₃ N ₄	0.1 M KOH	420	1.4	Free-standing film	Angew. Chem. Int. Ed. 2016, 55, 1138
cobalt-nitrogen-carbon	0.1 M KOH	440	0.28	GCE	Energy Environ. Sci. 2016, 9, 1661
N,O-dual doped graphene-CNT hydrogel film	0.1 M KOH	485	1.75	-	Adv. Mater. 2014, 26, 2925
nano porous carbon nanofiber films	0.1 M KOH	610	0.1	GCE	Adv. Mater. 2016, 28, 3000

- [S1] P. E. Blöchl, *Phys. Rev. B* 1994, **50**, 17953.
- [S2] G. Kresse and D. Joubert, *Phys. Rev. B* 1999, **59**, 1758.
- [S3] G. Kresse and J. Furthmüller, *Comput. Mater. Sci.* 1996, **6**, 15.
- [S4] G. Kresse and J. Furthmüller, *Phys. Rev. B* 1996, **54**, 11169.
- [S5] J. P. Perdew, K. Burke and M. Ernzerhof, *Phys. Rev. Lett.* 1996, **77**, 3865.
- [S6] I. C. Man, H.-Y. Su, F. Calle-Vallejo, H. A. Hansen, J. I. Martínez, N. G. Inoglu, J. Kitchin, T. F. Jaramillo, J. K. Nørskov and J. Rossmeisl, *ChemCatChem* 2011, **3**, 1159.
- [S7] Y. S. Wang, Z. M. Feng, S. Z. Yang, C. Gagnon, V. Gariépy, D. Laul, W. Zhu, R. Veillette, M. L. Trudeau, A. Guerfi and K. Zaghi, *J. Power Sources* 2018, **378**, 516.
- [S8] F. Cosandey, D. Su, M. Sina, N. Pereira and G. G. Amatucci, *Micron*. 2012, **43**, 22.
- [S9] Z. L. Wang, J. S. Yin and Y. D. Jiang, *Micron*. 2000, **31**, 571.